The Astrophysical Journal, 597:L89–L92, 2003 November 10

DETECTION OF THE INTEGRATED SACHS-WOLFE AND SUNYAEV-ZELDOVICH EFFECTS FROM THE COSMIC MICROWAVE BACKGROUND–GALAXY CORRELATION

Pablo Fosalba,[1] Enrique Gaztañaga,[2,3] and Francisco J. Castander[2]
Received 2003 July 19; accepted 2003 September 19; published 2003 October 20

ABSTRACT

We present a cross-correlation analysis of the *W ilkinson Microwave Anisotropy Probe* cosmic microwave background (CMB) temperature anisotropies and the Sloan Digital Sky Survey galaxy density fluctuations. We find significant detections of the angular CMB-galaxy correlation for both a flux-limited galaxy sample ($z \sim 0.3$) and a high-redshift ($z \sim 0.5$) color-selected sample. The signal is compatible with that expected from the integrated Sachs-Wolfe (ISW) effect at large angles ($\theta > 4°$) and the Sunyaev-Zeldovich (SZ) effect at small scales ($\theta < 1°$). The detected correlation at low z is in good agreement with a previous analysis using the Automated Plate Measuring survey ($z \sim 0.15$). The combined analysis of all three samples yields a total significance of better than 3 σ for the ISW effect and of about 2.7 σ for the SZ effect, with a Compton parameter $\bar{y} \simeq 10^{-6}$. For a given flat Λ cold dark matter model, the ISW effect depends on both the value of Ω_Λ and the galaxy bias b. To break this degeneracy, we estimate the bias using the ratio between the galaxy and mass autocorrelation functions in each sample. With our bias estimation, all samples consistently favor a best-fit dark-energy–dominated model: $\Omega_\Lambda \simeq 0.8$, with a 2 σ error $\Omega_\Lambda = 0.69$–0.86.

Subject headings: cosmic microwave background — cosmology: observations

On-line material: color figures

1. INTRODUCTION

A recent study (Fosalba & Gaztañaga 2003) has cross-correlated the cosmic microwave background (CMB) anisotropies measured by the *Wilkinson Microwave Anistropy Probe* (*WMAP*; Bennett et al. 2003) with galaxy fluctuations in the Automated Plate Measuring (APM) galaxy survey (Maddox et al. 1990) to find significant detections for both the integrated Sachs-Wolfe (ISW) effect and the thermal Sunyaev-Zeldovich (SZ) effect. The ISW detection is in agreement with other analyses based on X-ray and radio sources (Boughn & Crittenden 2003; Nolta et al. 2003), while Hernandez-Monteagudo & Rubino-Martin (2003) fail to detect the SZ effect when comparing *WMAP* with different optical cluster templates (see also Myers et al. 2003). It should be stressed nevertheless that cluster or galaxy group catalogs are too sparse and typically produce worse signal-to-noise ratios than galaxy surveys. Moreover, depending on the sample, there could be a significant cancellation of the ISW and SZ effects on scales smaller than a few degrees (see § 4). In this Letter, we cross-correlate the *WMAP* CMB temperature anisotropies with galaxies from the Sloan Digital Sky Survey (SDSS; York et al. 2000). When we were finishing this work, we became aware of a similar analysis (Scranton et al. 2003) that uses different color and photometric redshift-selected samples from the SDSS.

2. DATA

We make use of the largest data sets currently available to study the CMB-galaxy cross-correlation. In order to probe the galaxy distribution, we have selected subsamples from the first SDSS Data Release (SDSS DR1; Abazajian et al. 2003), which covers ~2000 deg^2 (i.e., 5% of the sky). The samples analyzed here have different redshift distributions and a large number of galaxies (10^5–10^6, depending on the sample). We concentrate our analysis on the north sky (~1500 deg^2, i.e., 3.6% of the sky) because it contains the largest and widest strips. The south sky of the SDSS DR1 (~500 deg^2) consists of three narrow and disjoint 2.°5 strips, which are less adequate for our analysis.

Our main sample, hereafter the SDSS all sample, includes all objects classified as galaxies with an extinction-corrected magnitude $r < 21$ and a low associated error (<20%). This sample contains ~5 million galaxies distributed over the north sky. Its predicted redshift distribution is broad and has a median redshift $\bar{z} \sim 0.3$. Our high-redshift sample (hereafter the SDSS high-z sample) comprises $\sim 3 \times 10^5$ galaxies, with $\bar{z} \sim 0.5$. It was selected by imposing magnitude cuts and color cuts perpendicular to the redshift evolution and the spectral type variations based on theoretical spectral synthesis models. We shall also compare our results with the APM analysis in Fosalba & Gaztañaga (2003), who used a $b_J = 17$–20 sample, $\bar{z} \simeq 0.15$, an area of ~4300 deg^2, and 1.2 million galaxies.

For the CMB data, we use the first-year full-sky *WMAP* maps (Bennett et al. 2003). Since the observed CMB-galaxy correlation is practically independent of the *WMAP* frequency band used (Fosalba & Gaztañaga 2003), we shall focus on the V band (~61 GHz) since it conveniently combines low pixel noise and high spatial resolution, 21′. In addition, we have also used the W band and a foreground “cleaned” *WMAP* map (Tegmark, de Oliveira-Costa, & Hamilton 2003) to check that our results are free of galactic contamination. We mask out pixels using the conservative Kp0 mask that cuts out 21.4% of the sky (Bennett et al. 2003). All the maps used have been digitized into 7′ pixels using HEALPix[4] (Górski, Hivon, & Wandelt 1999).

3. CROSS-CORRELATION AND STATISTICAL TESTS

We follow the notation introduced in Fosalba & Gaztañaga (2003). We define the cross-correlation function as the expec-

[1] Institut d’Astrophysique de Paris, 98bis Boulevard Arago, 75014 Paris, France.

[2] Institut d’Estudis Espacials de Catalunya/CSIC, Gran Capità 2-4, 08034 Barcelona, Spain.

[3] Insituto Nacional de Astrofísica Óptica y Electrónica, Tonantzintla, Puebla 7200, Mexico.

[4] See http://www.eso.org/science/healpix.

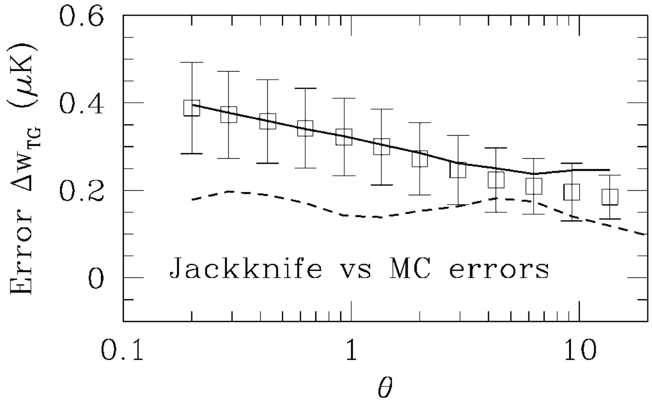

FIG. 1.—Errors in the cross-correlation $w_{T,G}(\theta)$ from the dispersion in 200 MC simulations (*solid line*) as compared with the mean and the dispersion (*squares with erro r bars*) in the JK error estimation over the same simulations. The dashed line correspond to the JK error in the real *WMAP*–SDSS all sample.

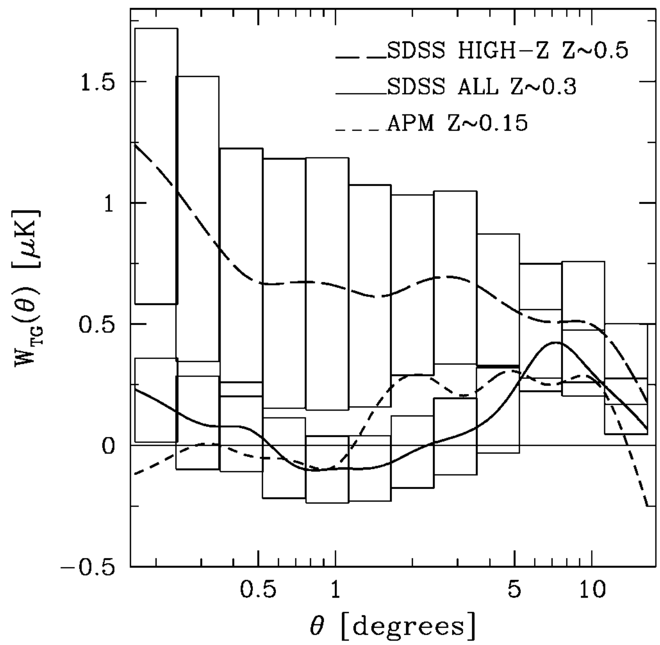

FIG. 2.—*WMAP*-SDSS correlation. The long-dashed line shows the measurement for the SDSS high-z sample, while the solid line displays the correlation for the SDSS all sample. For reference, the short-dashed line displays the same measurement using the APM galaxy survey instead of the SDSS. The boxes show 1 σ error bars. [*See the electronic edition of the Journal for a color version of this figure.*]

tation value of density fluctuations $\delta_G = N_G/\langle N_G\rangle - 1$ and temperature anisotropies $\Delta_T = T - T_0$ (in units of microkelvins) at two positions $\hat{\boldsymbol{n}}_1$ and $\hat{\boldsymbol{n}}_2$ in the sky: $w_{T,G}(\theta) \equiv \langle \Delta_T(\hat{\boldsymbol{n}}_1)\delta_G(\hat{\boldsymbol{n}}_2)\rangle$, where $\theta = |\hat{\boldsymbol{n}}_2 - \hat{\boldsymbol{n}}_1|$.

We compute the CMB-galaxy correlation and the associated statistical error bars using the jackknife (JK) method described in Fosalba & Gaztañaga (2003) and references therein. The survey is divided into $M = 16$ (we find similar results for $M = 8$) separate regions on the sky, each of equal area. The $w_{T,G}$ analysis is then performed M times, each time removing a different region, the so-called JK subsamples. The covariance C_{ij} for $w_{T,G}$ between scales θ_i and θ_j is obtained by rescaling the covariance of the JK subsamples by a factor $M - 1$ (see eq. [3] in Fosalba & Gaztañaga 2003). To test the JK errors and covariance, we have also run 200 *WMAP V*-band Monte Carlo (MC) realizations. We add random realizations of the measured *WMAP* temperature angular power spectrum (Bennett et al. 2003) to those of the white noise estimated for the relevant frequency band (Hinshaw et al. 2003). For each MC simulation, we estimate the mean "accidental" correlation $w_{T,G}$ of simulated CMB maps to the SDSS galaxy density fluctuation map. We also estimate the associated JK error in each MC simulation. Figure 1 compares the "true" sampling error from the dispersion of $w_{T,G}(\theta)$ in 200 MC simulations with the mean and the dispersion of the JK errors over the same simulations. The JK error gives an excellent estimate of the true error up to $\theta \simeq 5°$. On larger scales, it only underestimates the error by 10%–20%, which is hardly significant given the uncertainties.

Figure 2 shows $w_{T,G}(\theta)$ for the different samples together with the corresponding JK error. It turns out that the JK errors from the real *WMAP* sample are in some cases smaller (up to a factor of 2) than the JK errors (or sample-to-sample dispersion) from the MC simulations. Figure 1 shows, as a dashed line, the comparison for the SDSS all sample, which exhibits the largest discrepancy. This difference in error estimation is not totally surprising since the MC simulations do not include any physical correlations but use a CMB power spectrum that is valid for the whole sky and is not constrained to match the CMB power over the SDSS region. The JK errors provide a model-free estimation that is only subject to moderate (20%) uncertainty, while MC errors depend crucially on the model assumptions that go into the simulations. Despite these differences in the MC error estimation, the overall significance for the detection turns out to be similar, as explained in § 4.1.

We derive the significance of the detected correlation by taking into account the large (JK) covariance between neighboring (logarithmic) angular bins in survey subsamples (but see also § 4.1). Adjacent bins at large scales ($\theta > 4°$) are correlated at the $\simeq$80% level, dropping to $\simeq$40% for alternative bins. Bins at smaller scales are progressively more correlated. To assign a conservative significance for the detection (i.e., against $w_{T,G} = 0$), we estimate the minimum χ^2 fit for a constant $w_{T,G}$ and give the difference $\Delta\chi^2$ to the $w_{T,G} = 0$ null detection. For example, at scales $\theta = 4°$–$10°$, we find $w_{T,G} = 0.53 \pm 0.21$ μK for the SDSS high-z sample, $w_{T,G} = 0.26 \pm 0.13$ μK for the SDSS all sample, and $w_{T,G} = 0.35 \pm 0.13$ μK for the APM survey; in all cases, we give 1 σ error bars.

We find the largest significance in the CMB-galaxy correlation for the SDSS high-z sample: $\Delta\chi^2 = 9.1$ (i.e., a probability $P = 0.3\%$ of no detection) for $\theta < 10°$ (with $\chi^2_{\min} = 14.6$ for $w_{T,G} = 0.55$ μK with 11 degrees of freedom (dof), although the fit is only approximate as the signal drops with scale). In order to assess the significance levels for the ISW and SZ effects from the observed CMB-galaxy correlations, we shall first introduce model predictions.

4. COMPARISON WITH PREDICTIONS

The temperature of CMB photons is gravitationally redshifted as they travel through the time-evolving dark matter gravitational potential wells along the line of sight, from the last scattering surface $z_s = 1089$ to us, $z = 0$ (Sachs & Wolfe 1967). At a given sky position $\hat{\boldsymbol{n}}$, $\Delta T^{\rm ISW}(\hat{\boldsymbol{n}}) = -2 \times \int dz\, \dot{\Phi}(\hat{\boldsymbol{n}}, z)$, and for a flat universe, $\nabla^2\Phi = -4\pi G a^2 \rho_m \delta$ (see eq. [7.14] in Peebles 1980). In Fourier space, it reads $\Phi(k,z) = -3/2\Omega_m (H_0/k)^2 \delta(k,z)/a$, and thus

$$w_{T,G}^{\rm ISW}(\theta) = \langle \Delta_T^{\rm ISW} \delta_G \rangle = \int \frac{dk}{k} P(k) g(k\theta), \quad (1)$$

with $g(k\theta) = 1/2\pi \int dz\, W_{\rm ISW}(z) W_G(z) j_0(k\theta r)$, where the ISW window is $W_{\rm ISW} = -3\Omega_m (H_0/c)^2 \dot{F}(z)$, with $c/H_0 \simeq 3000$ h Mpc^{-1}, $\dot{F} = d(D/a)/dr = (H/c)D(f-1)$, and $f \simeq \Omega_m^{6/11}(z)$ quantifies the time evolution of the gravitational potential. The galaxy window function is $W_G \simeq b(z)D(z)\phi_G(z)$, which depends on the galaxy bias, the linear dark matter growth, and the galaxy selection function. The ISW predictions for the three samples are shown in bottom panel of Figure 3. Unless stated otherwise, we use the concordance Λ cold dark matter (CDM) model with $\Omega_m = 0.3$, $\Omega_\Lambda = 0.7$, $\Gamma \simeq h\Omega_m = 0.2$, and $\sigma_8 = 1$.

The weak lensing effect prediction is quite similar to the ISW effect; we just need to replace the time derivative of the Newtonian potential by its two-dimensional Laplacian (Seljak & Zaldarriaga 2000), with $W_{\rm lens} = 3k^2\Omega_m (H_0/c)^2 (D/a)/d(r)$ $d(r)$ being the angular distance to the lensing sources [with $d(r_s - r)/d(r_s) \simeq 1$].

For the thermal SZ effect, we assume that the gas pressure $\delta_{\rm gas}$ fluctuations are traced by the galaxy fluctuations $\delta_{\rm gas} \simeq b_{\rm gas}\delta_G$ with a relative amplitude given by the gas bias, $b_{\rm gas} \simeq 2$, representative of galaxy clusters, although $b_{\rm gas}$ is uncertain to within 50% on linear scales and for low-z sources (Refregier & Teyssier 2002). A simple conservative estimate of the SZ effect is given by (Refregier, Spergel, & Herbig 2000)

$$w_{T,G}^{\rm SZ}(\theta) = -b_{\rm gas}\overline{\Delta T} w_{G,G}(\theta), \quad (2)$$

where $\overline{\Delta T}$ is the mean temperature change in CMB photons Compton-scattered by electrons in hot intracluster gas. Following Refregier et al. (2000), we calculate $\overline{\Delta T} = j(x)\bar{y}T_0$, where $T_0 \simeq 2.73$ K is the mean CMB temperature, $\bar{y}$ is the mean Compton parameter induced by galaxy clusters, and $j(x) = -4.94$ is the negative SZ spectral factor for the V band. The Compton parameter can be calculated by integrating along the line of sight the normalized galaxy redshift distribution convolved with the volume-averaged density-weighted temperature. The latter is obtained from the mass function and the M-T relation. We assume the Seth & Tormen mass function (Sheth & Tormen 1999; Sheth, Mo, & Tormen 2001) and the M-T relation given by Borgani et al. (1999). In summary, for the *WMAP* V band, we obtain $\overline{\Delta T} = 6.65$ μK for the SDSS all sample and $\overline{\Delta T} = 6.71$ μK for the SDSS high-z sample, which correspond to $\bar{y} \simeq 1.35 \times 10^{-6}$ for both samples. The SZ predictions for the three samples are shown in the bottom panel of Figure 3. Note that the galaxy autocorrelation explains most of the differences observed.

The total predicted correlation is thus the sum of three terms: the ISW, thermal SZ, and lensing contributions, $w_{T,G} = w_{T,G}^{\rm ISW} + w_{T,G}^{\rm SZ} + w_{T,G}^{\rm lens}$. Figure 3 shows individual contributions of these effects (*bottom panel*) and the total (*top panel*) for the three samples analyzed. The ISW effect typically dominates for angles $\theta > 4°$, while the SZ effect is expected to be significant on small scales ($\theta < 1°$). Lensing is found to be negligible at all scales for our samples.

Before we can make a direct comparison between theory and observations, we shall address the issue of galaxy bias. The higher redshift sample requires a high bias ($b > 1$) to explain the large cross-correlation seen at all scales (the SZ effect being smaller at high redshift). At low redshifts, the measured correlation is dominated by the thermal SZ effect on small scales ($\theta < 1°$) and by ISW effect on large scales ($\theta > 4°$). Here no bias is required to match the observations. This agrees quite well with our self-consistent bias estimation: for each sample, we can estimate the ratio $b^2 \simeq w_{G,G}/w_{M,M}$, where $w_{M,M}$ and $w_{G,G}$ are the (theoretically predicted) matter and (measured) galaxy autocorrelation functions. For the APM and SDSS all samples, we find $b^2 \simeq 1$, while for the SDSS high-z sample, we get $b^2 \simeq 6$.

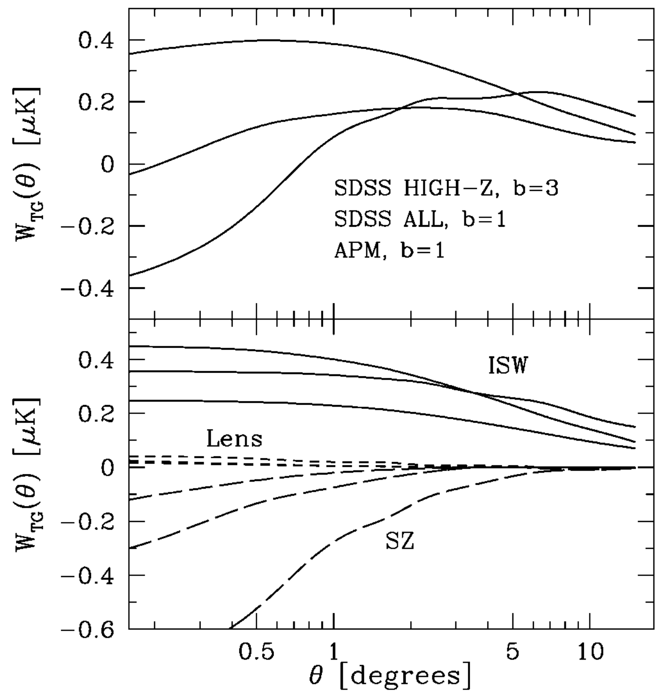

FIG. 3.—Theoretical predictions. In the bottom panel, the solid, long-dashed, and short-dashed lines show the ISW, SZ, and lensing predictions. Different sets of lines correspond to the APM, SDSS all, and SDSS high-z samples. *Top panel*: Total prediction (ISW+SZ+lensing) for the three samples. We have assumed a ΛCDM model with a fixed $b_{\rm gas} = 2$ in all cases, $b = 3$ for the SDSS high-z sample and $b = 1$ for the APM and SDSS all samples. [*See the electronic edition of the Journal for a color version of this figure.*]

4.1. *Significance Tests*

ISW effect.—On large scales ($\theta > 4°$), the ISW effect is expected to dominate for all survey depths (see Fig. 3). Therefore, from the large-angle CMB-galaxy correlation, we can directly infer the ISW effect (i.e., $w_{T,G} = w_{T,G}^{\rm ISW}$; see the end of § 3). In particular, for the SDSS high-z sample, a constant correlation fit rejects the null detection with high significance: $\Delta\chi^2 = 6.0$ ($P = 1.4\%$), comparable to the level found for the APM survey, $\Delta\chi^2 = 6.1$ ($P = 1.3\%$). A smaller significance is obtained for the SDSS all sample: $\Delta\chi^2 = 3.9$ ($P = 4.8\%$). Alternatively, we can use the uncorrelated MC simulations (see § 3) to get an independent estimate of the significance. When a particular MC simulation has an accidentally large value of $w_{T,G}$, it also has a large associated JK error. We can thus assign a significance to our measurement by asking how many of the 200 MC simulations have a value of $w_{T,G}$ equal to or larger than the observations with an associated JK error equal to or smaller than that found for the observations. We find that only two of the MC simulations fulfil this condition in any of the samples, meaning that the significance of each detection is better than 1% (for each of the three different data samples).

Since these samples are basically independent, we can combine them to infer a total significance for the ISW detection: we find a total $\Delta\chi^2 = 16$ ($P = 0.1\%$ for 3 dof) corresponding to 3.3 σ. Note we could do better by using a (scale-dependent) ΛCDM model theory prediction, but at the cost of introducing model-dependent detection levels. Moreover, we can further include the ISW-dominated small-angle bins in our deepest sample, where the SZ effect is negligible, increasing the significance to $\Delta\chi^2 = 18.8$ ($P = 0.03\%$ for 3 dof); i.e., we detect the ISW effect at the a 3.6 σ level.

SZ effect.—We can estimate the significance of the drop in the signal at small angles in the SDSS all and APM samples due to the SZ effect (see Fig. 3) using the best-fit constant at large angles (i.e., the ISW signal), and we can ask for the observed deviation from such value at smaller scales. For $\theta < 1°$, we find $w_{T,G}^{SZ} = -0.27 \pm 0.11$ for SDSS all sample and $w_{T,G}^{SZ} = -0.41 \pm 0.16$ for the APM sample (1 σ error bars). Note that this is conservative because the ISW effect increases slightly as we approach smaller scales (see § 4). This test gives $\Delta\chi^2 = 5.5$ ($P = 2\%$) for the SDSS all sample and $\Delta\chi^2 = 8.5$ ($P = 0.3\%$) for the APM sample.

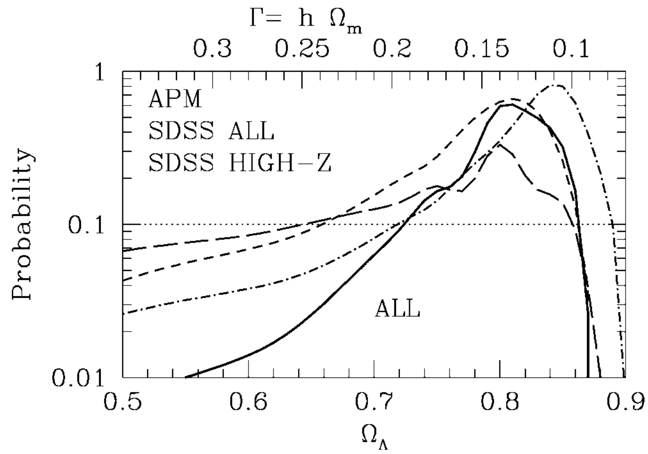

FIG. 4.—Estimating dark energy. The long-dashed, short-dashed, and dot-dashed lines show the probability distribution for Ω_Λ in the SDSS all, APM, and SDSS high-z samples. The combined distribution (for 3 dof) is shown by the solid line. [*See the electronic edition of the Journal for a color version of this figure.*]

5. DISCUSSION

We have measured the CMB-galaxy correlation using *WMAP* and the SDSS DR1 galaxy survey. We measure a significant cross-correlation at low ($z \sim 0.3$) and high ($z \sim 0.5$) redshifts. We detect a positive correlation on large scales induced by the ISW effect at the 2 σ level for the (broadly distributed) low-z sample. This correlation is similar to that measured for the lower redshift ($z \sim 0.15$) APM galaxies (Fosalba & Gaztañaga 2003), although the latter has a larger significance, 2.5 σ. Moreover, the significance of the detection rises to 3 σ for the SDSS high-z sample. The combined analysis for the three samples gives a 3.6 σ significance (see § 4.1).

Our measurements at large scales are in good agreement with ISW predictions for a dark-energy–dominated universe. Figure 4 shows the probability distribution for Ω_Λ in a flat ΛCDM model. We have fixed $\sigma_8 = 1$, $h = 0.7$, and $\Omega_M + \Omega_\Lambda = 1$. As we vary Ω_Λ, the shape parameter for the linear power spectrum $P(k)$ consistently changes, $\Gamma = h\Omega_M$ (Bond & Efstathiou 1984). We only use the data for $\theta > 4°$, where the ISW effect is the dominant contribution. We fix the bias b by comparing the matter angular autocorrelation function in each model with the galaxy autocorrelation in each sample. We find $b \simeq 1$ for the APM and SDSS all samples and $b \simeq \sqrt{6}$ for the SDSS high-z sample. The $\Delta\chi^2$ value in each model refers to the minimum χ^2 fit to a constant in the range $4° < \theta < 10°$. As can be seen in the figure, all the samples prefer large values of Ω_Λ, with the best fit $\Omega_\Lambda \simeq 0.8$ with a 2 σ range $\Omega_\Lambda = 0.69$–0.87.

We also see evidence (2.7 σ level) of the thermal SZ effect from the drop of the CMB-galaxy correlation on small scales in the low-z samples of SDSS and APM galaxies. These new measurements can be used to constrain the redshift evolution of the physical properties of gas inside galaxy clusters.

P. F. wants to thank Francois Bouchet for useful suggestions. F. J. C. acknowledges useful discussions with Andy Connolly. We acknowledge support from the Barcelona-Paris bilateral project (Picasso Programme). P. F. acknowledges a postdoctoral CMBNet fellowship from the EC. E. G. and F. J. C. acknowledge the Spanish MCyT, project AYA2002-00850, EC-FEDER funding.

REFERENCES

Abazajian, K., et al. 2003, AJ, 126, 2081
Bennett, C. L., et al. 2003, ApJS, 148, 1
Bond, J. R., & Efstathiou, G. 1984, ApJ, 285, L45
Borgani, S., Rosati, P., Tozzi, P., & Norman, C. 1999, ApJ, 517, 40
Boughn, S. P., & Crittenden, R. G. 2003, preprint (astro-ph/0305001)
Fosalba, P., & Gaztañaga, E. 2003, Phys. Rev. Lett., submitted (astro-ph/0305468)
Górski, K. M., Hivon, E., & Wandelt, B. D. 1999, in Proc. MPA-ESO Conf., Evolution of Large Scale Structure: From Recombination to Garching, ed. A. J. Banday, R. K. Sheth, & L. A. N. da Costa (Enschede: PrintPartners Ipskamp), 37
Hernandez-Monteagudo, C., & Rubino-Martin, J. A. 2003, MNRAS, in press (astro-ph/0305606)
Hinshaw, G., et al. 2003, ApJS, 148, 63
Maddox, S. J., Efstathiou, G., Sutherland, W. J., & Loveday, J. 1990, MNRAS, 242, 43P
Myers, A. D., Shanks, T., Outram, P. J., & Wolfendale, A. W. 2003, MNRAS, submitted (astro-ph/0306180)
Nolta, M. R., et al. 2003, ApJ, submitted (astro-ph/0305097)
Peebles, P. J. E. 1980, The Large-Scale Structure of the Universe (Princeton: Princeton Univ. Press)
Refregier, A., Spergel, D. N., & Herbig, T. 2000, ApJ, 531, 31
Refregier, A., & Teyssier, R. 2002, Phys. Rev. D, 66, 043002
Sachs, R. K., & Wolfe, A. M. 1967, ApJ, 147, 73
Scranton, R., et al. 2003, Phys. Rev. Lett., submitted (astro-ph/0307335)
Seljak, U., & Zaldarriaga, M. 2000, ApJ, 538, 57
Sheth, R. K., Mo, H. J., & Tormen, G. 2001, MNRAS, 323, 1
Sheth, R. K., & Tormen, G. 1999, MNRAS, 308, 119
Tegmark, M., de Oliveira-Costa, A., & Hamilton, A. 2003, preprint (astro-ph/0302496)
York, D. G., et al. 2000, AJ, 120, 1579